J Mater Sci (2021) 56:305–312

Ceramics

Theoretical study of the phase transitions and electronic structure of ($Zr_{0.5}$, $Mg_{0.5}$)N and ($Hf_{0.5}$, $Mg_{0.5}$)N

M. A. Gharavi[1,*], R. Armiento[2], B. Alling[2], and P. Eklund[1]

[1] Thin Film Physics Division, Department of Physics, Chemistry and Biology (IFM), Linköping University, 581 83 Linköping, Sweden
[2] Theoretical Physics Division, Department of Physics, Chemistry and Biology (IFM), Linköping University, 581 83 Linköping, Sweden

Received: 8 July 2020
Accepted: 19 September 2020
Published online: 1 October 2020

ABSTRACT

Rock-salt scandium nitride has gained interest due to its thermoelectric properties including a relatively high Seebeck coefficient. This motivates research for other semiconductor materials that exhibit similar electronic structure features as ScN. Using density functional theory calculations, we have studied disordered solid solutions of ($Zr_{0.5}$, $Mg_{0.5}$)N and ($Hf_{0.5}$, $Mg_{0.5}$)N using the special quasi-random structure model. The results show that within a mean-field approximation for the configurational entropy, the order–disorder phase transformation between the monoclinic $LiUN_2$ prototype structure and the rock-salt cubic random alloy of these mentioned solid solutions occur at 740 K and 1005 K for ($Zr_{0.5}$, $Mg_{0.5}$)N and ($Hf_{0.5}$, $Mg_{0.5}$)N, respectively. The density-of-states for the two ternary compounds is also calculated and predicts semiconducting behavior with band gaps of 0.75 eV for ($Zr_{0.5}$, $Mg_{0.5}$)N and 0.92 eV for ($Hf_{0.5}$, $Mg_{0.5}$)N. The thermoelectric properties of both compounds are also predicted. We find that in the range of a moderate change in the Fermi level, a high Seebeck coefficient value at room temperature can be achieved.

Introduction

The aim to decrease reliance on fossil fuels has led to research on energy harvesting, for example of thermal and solar energy. Thermoelectrics, the process in which thermal gradients can be transformed into an external voltage, is particularly useful when a long-lasting and maintenance-free power source is needed [1–3]. In addition to a high Seebeck coefficient and electrical conductivity, features such as chemical stability, non-toxicity and ease of manufacturing are of importance when choosing an appropriate thermoelectric material.

Transition metal nitrides are known for the above properties and have been studied extensively due to hardness, temperature resistance, mechanical and

Handling Editor: David Cann.

Address correspondence to E-mail: mohammad.amin.gharavi@liu.se

https://doi.org/10.1007/s10853-020-05372-1

chemical stability [4]. Among the d-block nitrides, cubic chromium nitride (CrN) [5, 6] and cubic scandium nitride (ScN) exhibit interesting thermoelectric properties [7–11]. In addition to its chemical, thermal and mechanical stability, ScN has a relatively large Seebeck coefficient (reaching −180 μV/K at 800 K). When including its low electrical resistivity, large power-factors between 2.5 and 3.5 × 10^{-3} Wm^{-1} K^{-2} have been reported [12, 13]. Furthermore, ScN can also become *p*-type by Sc-site doping [14, 15]. However, ScN does have a relatively large thermal conductivity [16–19] of approximately 8–12 Wm^{-1} K^{-1} which will reduce the thermoelectric efficiency and make it an impractical thermoelectric material in pure form.

Previously, Alling [20] addressed this issue by proposing a ternary nitride mimicking the features of ScN. Scandium (which is a group-3 element) can be replaced with one group-2 and one group-4 element in a 50/50 proportion to obtain the same electron valence. The final compound should then have a $MeAEN_2$ stoichiometry, with *Me* representing a transition metal from the group-4 elements and *AE* belonging to the group-2 (alkaline earth) elements, such as magnesium. The study focused on $TiMgN_2$, and it was predicted to be stable using density functional theory (DFT). Band structure calculations predicted stoichiometric $TiMgN_2$ to have a 1.11 eV band gap using the HSE06 [21] hybrid functional and 0.22 eV with the PBE GGA functional known to give band gaps that are smaller than the experimental values. The SQS model was also used to study (Ti_x, Mg_{1-x})N solid solutions where ($Ti_{0.5}$, $Mg_{0.5}$)N was shown to be a non-magnetic semiconductor with a predicted 1.33 eV band gap. These results were also supported by Irokawa and Usami [22]. An attempt to synthesize ($Ti_{0.5}$, $Mg_{0.5}$)N by magnetron sputtering was conducted by Wang and Gall [23, 24]. In their study, they found a negative temperature coefficient of resistivity and a vanishing density-of-states at the Fermi level measured by X-ray photoelectron spectroscopy, showing that ($Ti_{0.5}$, $Mg_{0.5}$)N is a semiconductor. In a separate study by the present authors, ($Ti_{0.5}$, $Mg_{0.5}$)N was determined to have a Seebeck coefficient value of -25 μV/K [25]. It was also shown that at approximately 800 °C, high-resolution scanning transmission electron microscopy (HR-STEM) shows that the rock-salt cubic random alloy of ($Ti_{0.5}$, $Mg_{0.5}$)N goes through a phase transformation at the grain boundaries, forming a quaternary ($Ti_{0.5}$, $Mg_{0.5}$)N_xO_y superstructure when oxygen is also present. Kim et al. [26] used hydrogen gas as a means to control the oxygen content in the grain boundaries of (Mg, Zr) oxynitride thin films, which in return can be used to tailor the optoelectronic properties of such films.

In a previous paper, we expanded the research on this group of compounds by studying the phase stability and band structure of $ZrMgN_2$ and $HfMgN_2$ [27]. It was shown that the stoichiometric compositions have an almost equal tendency to crystallize in both the $NaCrS_2$ superstructure and the $LiUN_2$ prototype monoclinic structures. $ZrMgN_2$ shows a 0.89 eV indirect band gap when crystallizing into the $NaCrS_2$ structure while as crystallization into the $LiUN_2$ structure results in a 0.46 eV direct band gap. As for $HfMgN_2$, the band gap increases as crystallization into $NaCrS_2$ results in a 1.19 eV indirect band gap and crystallization into $LiUN_2$ results in a 0.77 eV direct band gap. Predicted thermoelectric properties of the semiconducting compounds showed that in the range of a moderate change in the Fermi level, high room temperature Seebeck coefficient values can be achieved. Experimental synthesis of $Mg_xZr_{2-x}N_2$ by Bauers et al. [28] showed that Zr-rich samples are more metallic, while Mg-rich samples are more insulating, which shows a degree of tunability of the electrical properties.

In the present paper, we investigate the configurationally disordered solid solutions ($Zr_{0.5}$, $Mg_{0.5}$)N and ($Hf_{0.5}$, $Mg_{0.5}$)N using the special quasi-random structure (SQS) method in conjunction with DFT calculations. By comparing the formation energy of the disordered alloys of ($Zr_{0.5}$, $Mg_{0.5}$)N and ($Hf_{0.5}$, $Mg_{0.5}$)N in the rock-salt cubic structure with that of its $LiUN_2$ ordered structure counterparts, the order/disorder transition temperature can be calculated within a mean-field approximation. The density-of-states of ($Zr_{0.5}$, $Mg_{0.5}$)N and ($Hf_{0.5}$, $Mg_{0.5}$)N are also studied, and these calculations are used to predict their energy band gap and thermoelectric properties.

Computational details

First-principles calculations were performed using DFT [29, 30] with the projector augmented wave method (PAW) [31] implemented in the Vienna ab initio simulation package (VASP) [32–34] version 5.2. Electronic exchange–correlation effects and the

electronic band structure were modeled with the generalized gradient approximation (GGA) using the Perdew–Burke–Ernzerhof (PBE) functional [35]. It should be noted that the Kohn–Sham band gaps of standard GGA calculations are systematically smaller than experimental band gaps, but for the present work, this is not an issue since we are mostly concerned with screening candidate materials and dismissing metallic compounds. The plane wave energy cutoff was set at 600 eV. The required structure files for the crystal structures were obtained using the special quasi-random structures (SQS) method [36] for the DFT calculations. The SQS unit cell is presented by 128 atoms and all internal atomic positions were fully relaxed while the cell shape is kept at the rock-salt cubic structure. These SQS structures were previously used to model $Zr_{1-x}Gd_xN$ and $Hf_{1-x}Gd_xN$ [37]. The density-of-states (DoS) illustrations are prepared by the high-throughput toolkit (httk) [38] and the 3D rendering of the crystal structure by VESTA [39]. For the order/disorder phase transformation temperature, the formation energy per formula unit was calculated for each ternary compound and related to the competing $LiUN_2$ ordered structure.

The present work uses the same correction of the N_2 energy as used in the Materials Project, based on work by Wang et al. [40] as standard GGA exchange–correlation functionals in DFT which are known to, in general, have systematic errors in the prediction of energy differences between solid and gas phase systems [41]. Hence, to accurately reproduce the formation energy of a system relative to a gas endpoint, it is common to adjust the gas phase energy.

The calculations of SQS structures used a $4 \times 4 \times 4$ k-point mesh for Brillouin zone sampling and were executed with the Monkhorst–Pack scheme [42]. For density-of-states (DoS) calculations, the tetrahedron method was used in order to obtain band gap values [43].

Finally, the Seebeck coefficient S and power-factor $S^2\sigma\tau^{-1}$ (τ being the charge carrier relaxation time) of the predicted semiconductors are calculated at room temperature and 600 K as functions of the chemical potential using Boltzmann transport theory with the constant relaxation time approximation. We use the software BoltzTraP [44] on DFT calculations with a $7 \times 7 \times 7$ k-point mesh for Brillouin zone sampling.

Results and discussion

Figure 1 shows the three-dimensional rendering of the $(Me_{0.5}, AE_{0.5})N$ compound based on the SQS model, where *Me* is either zirconium or hafnium and *AE* is an alkaline earth element, in this case magnesium. In order to relax the unit cell, the lattice parameter of the cubic unit cell was calculated starting from an estimate from Vegard's law. The calculated lattice parameter for ZrN, HfN and MgN is reported to be 4.618 Å, 4.538 Å [45] and 4.440 Å [41], respectively. Thus, (Zr, Mg)N and (Hf, Mg)N compounds with a 50/50 metal atom ratio would have a lattice parameter of 4.529 Å and 4.489 Å according to Vegard's law. Cell relaxation was done by plotting the energy of the primitive cell versus the lattice parameter obtained from Vegard's law in steps of ± 0.05 Å and ± 0.10 Å. A Gaussian fit of the resulting curve was then used to predict the lattice parameter leading to values of 4.556 Å and 4.508 Å. Both curves are shown in Fig. 2a and b.

To calculate the order/disorder phase transition temperature, the formation energy of the $(Me_{0.5}, AE_{0.5})N$ random alloy, based on the calculated optimal lattice parameter, is compared to its ordered structure, the $LiUN_2$ superstructure which was studied previously [27]. According to the thermodynamic stability criteria at constant pressure and temperature, the Gibbs free energies at the transition temperature, T_C satisfy:

$G^{ord} = G^{dis}$, where G^{ord} and G^{dis} are the Gibbs free energy of the ordered and disordered structures, respectively. At zero pressure, using the

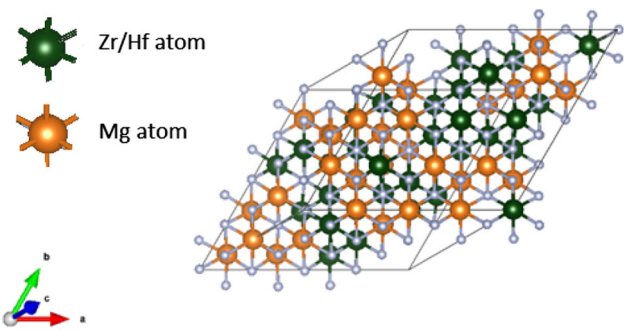

Figure 1 Unit cell of the $(Me_{0.5}, AE_{0.5})N$ compound based on the SQS model. The light orange colored spheres represent magnesium atoms, while the dark green colored spheres represent either zirconium or hafnium. The smaller grey colored spheres are nitrogen atoms.

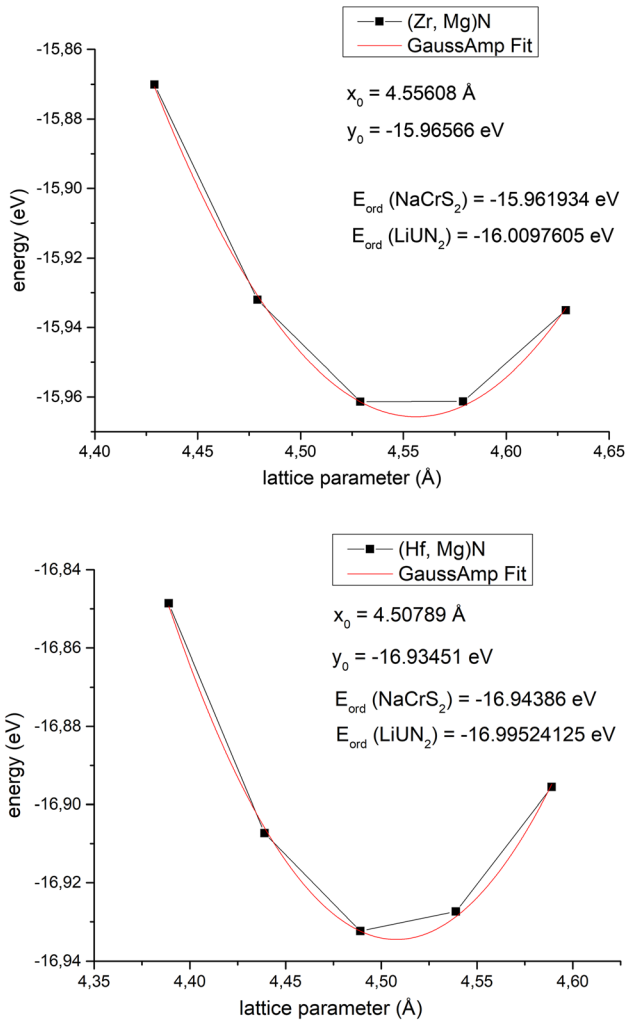

Figure 2 Gaussian fit of the energy vs lattice parameter for ($Zr_{0.5}$, $Mg_{0.5}$)N (top) and ($Hf_{0.5}$, $Mg_{0.5}$)N (bottom). Data points are based on Vegard's law.

approximation that the ordered phase is described by an ideally ordered structure, the above equation becomes:

$$E^{\text{ord}} = E^{\text{dis}} - T_C^S$$

and thus:

$$T_C = \frac{E^{\text{dis}} - E^{\text{ord}}}{S}$$

where T_C is the transition temperature and S is the entropy of the disordered random alloy. For the approximation that the disordered phase can be described by an ideal random alloy, usually called the mean-field approximation, its configurational entropy per formula unit, that is per metal atom, is given as:

$$S = -k_B[x \ln x + (1-x)\ln(1-x)]$$

where $x = 0.5$ is the metal atom ratio in our case and k_B is the Boltzmann constant. Table 1 provides the lattice parameters, formation energy of the disordered structure, $LiUN_2$ ordered structure energy and calculated transition temperature. Note that the mean-field approximation is known to overestimate the real configurational transition. As an example, the mean-field transition temperature for ordering in ($Ti_{0.5}$, $Mg_{0.5}$)N was found to be 1272 K while a full scale cluster expansion followed by Monte Carlo simulations obtained 950 K or 75% of the mean-field value [20]. As the respective mean-field transition temperatures are predicted to be 740 K and 1005 K for (Zr, Mg)N and (Hf, Mg)N, respectively, any prospective as-deposited atoms for sample synthesis will more than likely "freeze" on impact and the samples resulting a random solid solution in the NaCl structure (possibly with some short-range-order). Thus, high temperature annealing would be required for allowing diffusion and structure ordering, keeping the annealing temperature below T_C, a combination that ought to be challenging and motivates our further studies of the disordered structure below.

The density-of-states of both ($Zr_{0.5}$, $Mg_{0.5}$)N and ($Hf_{0.5}$, $Mg_{0.5}$)N are shown in Fig. 3. In both compounds, an energy gap can be seen at the Fermi level, with band gap values of 0.75 eV and 0.92 eV, respectively. These are somewhat larger than the value of 0.22 eV obtained with the PBE functional for the same 128-atom SQS in the ($Ti_{0.5}Mg_{0.5}$)N system [20]. As the Seebeck coefficient is related to the slope of the density-of-states near the Fermi level [46], calculating the thermoelectric properties becomes of interest. Figure 4 compares the Seebeck coefficient of ($Zr_{0.5}$, $Mg_{0.5}$)N and ($Hf_{0.5}$, $Mg_{0.5}$)N at 300 K and 600 K. The results show high Seebeck coefficient values exceeding ± 1000 μV/K at room temperature (comparable to that of an insulator). However, at these values, the electrical conductivity is close to zero. On the other hand, in the range of a moderate change in the Fermi level (i.e., moderate doping), a relatively high Seebeck coefficient value resulting in a notable power-factor becomes achievable. Figure 5 compares the power-factor of ($Zr_{0.5}$, $Mg_{0.5}$)N and ($Hf_{0.5}$, $Mg_{0.5}$)N at 300 K and 600 K. The predicted power-factor is, however, divided by the relaxation

Table 1 Order/disorder transition temperature for ($Zr_{0.5}$, $Mg_{0.5}$)N and ($Hf_{0.5}$, $Mg_{0.5}$)N

Compound	Lattice parameter	Ordered ($LiUN_2$) energy	Disordered (alloy) energy	Order/disorder transition temp
(Zr, Mg)N	4.556 Å	−16.010 eV	−15.966 eV	740 K
(Hf, Mg)N	4.508 Å	−16.995 eV	−16.935 eV	1005 K

Calculation based on random alloy energy and the $LiUN_2$ ordered structure energy

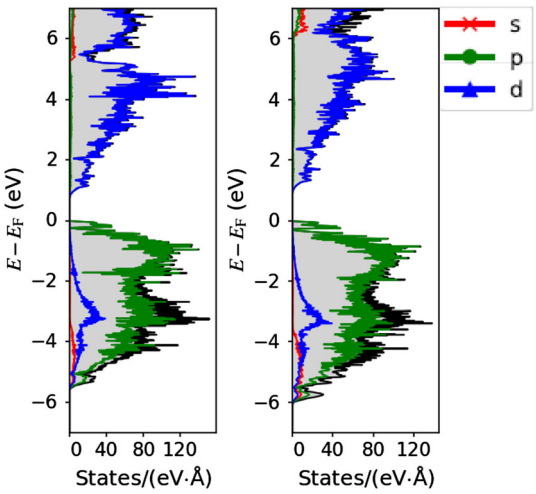

Figure 3 Density-of-states for ($Zr_{0.5}$, $Mg_{0.5}$)N (left) and ($Hf_{0.5}$, $Mg_{0.5}$)N (right). Band gap values are calculated to be 0.75 eV and 0.92 eV, respectively.

of pure ScN, but possibly with a lower thermal conductivity value as it would be expected from a disordered alloy [47] between heavy elements such as zirconium or hafnium and a light element like magnesium. Please note that multivalent ternaries likely have different charge density distributions around the cations compared to binaries, and thus have different scattering physics. As a result, our assumption will only give a rough estimate until actual samples are characterized.

Thus, our results for (Zr, Mg)N and (Hf, Mg)N solid solutions motivate additional experimental research of these compounds and comparison with theory [48, 49]. In both ordered and disordered structures, the studied magnesium-based transition metal nitrides show semiconducting and thermoelectric properties. The predicted band gap, however,

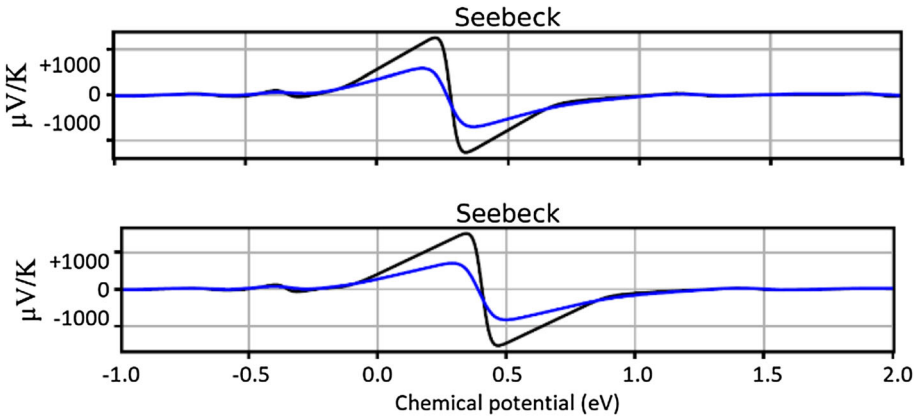

Figure 4 Seebeck coefficient value versus chemical potential of ($Zr_{0.5}$, $Mg_{0.5}$)N (top) and ($Hf_{0.5}$, $Mg_{0.5}$)N (bottom) at 300 K (black line) and 600 K (blue line). These calculations predict that the Seebeck coefficient value will decrease with the temperature.

time. This value is obtained from experimental data and is thus difficult to calculate theoretically. However, as our compounds are modeled after cubic ScN, using experimental data from Burmistrova et al. [16] and the classical equation for conductivity ($\sigma = ne^2\tau m^{-1}$), the constant relaxation time for ScN is estimated to be equal to 6.5×10^{-14} s. An estimated power-factor at room temperature would then be between 2.5 and 3.5×10^{-3} $Wm^{-1}K^{-2}$, similar to that is underestimated compared to experimental data (as expected), and the calculated Seebeck coefficient is that of an insulator and requires doping levels similar to their measured carrier densities to be a semiconductor. In both cases, increasing the temperature predicts a decrease in the Seebeck coefficient. On the other hand, the electric conductivity (and consequently, the power-factor) is predicted to increase as expected in semiconductors, although ordered crystals show less resistivity compared to disordered

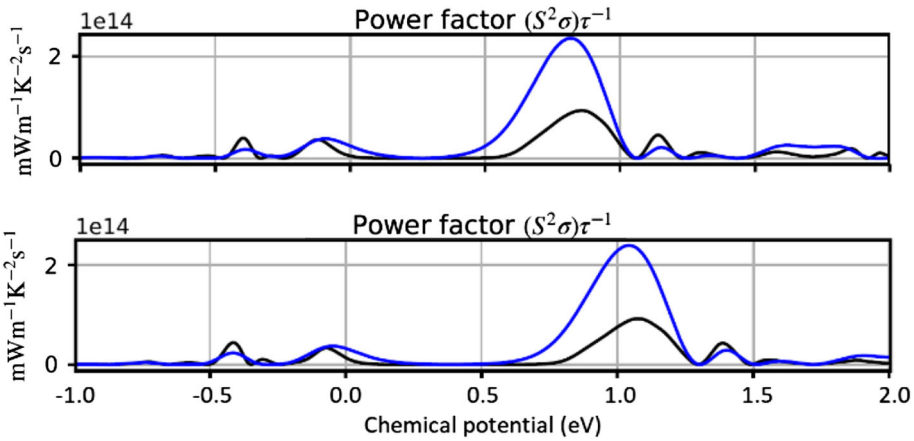

Figure 5 Power-factor/relaxation time value versus chemical potential of ($Zr_{0.5}$, $Mg_{0.5}$)N (top) and ($Hf_{0.5}$, $Mg_{0.5}$)N (bottom) at 300 K (black line) and 600 K (blue line). These calculations predict that the conductivity will increase with temperature, as expected for semiconducting material.

structures. Synthesis of the ordered structures could potentially be done by low temperature magnetron sputtering thin film deposition, resulting in the disordered phase, followed by high-temperature annealing of the disordered phase in a nitrogen gas environment as a means for cation lattice ordering [50].

Conclusion

Rock-salt solid solutions of ($Zr_{0.5}$, $Mg_{0.5}$)N and ($Hf_{0.5}$, $Mg_{0.5}$)N alloys have been studied by DFT calculations using the SQS method. The mean-field simulation shows that the order–disorder phase transformation between the monoclinic $LiUN_2$ prototype structure and the rock-salt cubic random alloy of the mentioned solid solutions occurs at 740 °C and 1005 °C, respectively. Together, with the low bulk diffusivities in nitrides, this highlights the importance of the disordered phases for ($Zr_{0.5}$, $Mg_{0.5}$)N and ($Hf_{0.5}$, $Mg_{0.5}$)N grown at normal PVD temperatures. The density-of-states for the two ternary nitride alloys are also calculated and predict semiconducting behavior with a PBE-GGA band gap of 0.75 eV and 0.92 eV. Seebeck coefficient and power-factors are also predicted, showing that in the range of a moderate change in the Fermi level, high room-temperature power-factor values can be achieved. Similar to previous theoretical studies on $TiMgN_2$ which motivated research and synthesis of ($Ti_{0.5}$, $Mg_{0.5}$)N and showing that materials semiconducting and thermoelectric properties, the theoretical predictions regarding the properties of (Zr, Mg)N and (Hf, Mg)N solid solutions motivate additional experimental research and the actual synthesis of these nitride alloys.

Acknowledgements

The authors acknowledge funding from the Swedish Government Strategic Research Area in Materials Science on Functional Materials at Linköping University (Faculty Grant SFO-Mat-LiU No. 200900971), the Swedish Foundation for Strategic Research (SSF) through the Future Research Leaders 5 and 6 programs, the Knut and Alice Wallenberg foundation through the Academy Fellow program and the Swedish Research Council (VR) under Project Nos. 2016-03365, 330-2014-6336, 2016-04810, 2019-05403 and the Swedish e-Science Research Centre (SeRC). Also, the Marie Sklodowska Curie Actions, Cofund, Project INCA 600398, is gratefully acknowledged. The computations were enabled by resources provided by the Swedish National Infrastructure for Computing (SNIC) at the National Supercomputer Center (NSC) partially funded by the Swedish Research Council through grant agreement no. 2016-07213.

Funding

Open access funding provided by Linköping University.

References

[1] Yang J, Caillat T (2006) Thermoelectric materials for space and automotive power generation. MRS Bull 31:224–229

[2] He J, Tritt TM (2017) Advances in thermoelectric materials research: looking back and moving forward. Science 357:1369

[3] Beretta D et al (2019) Thermoelectrics: from history, a window to the future. Mater Sci Eng R Rep 138:10051

[4] Oyama ST (1996) Chemistry of transition metal carbides and nitrides. Springer, Heidelberg.

[5] Quintela CX, Podkaminer JP, Luckyanova MN, Paudel TR, Thies EL, Hillsberry DA, Tenne DA, Tsymbal EY, Chen G, Eom CB, Rivadulla F (2015) Epitaxial CrN thin films with high thermoelectric figure of merit. Adv Mater 27:3032–3037

[6] Febvrier A, Pallier C, Eklund P (2018) Microstructure and thermoelectric properties of CrN and CrN/Cr_2N thin films. J Phys D Appl Phys 51:355302.

[7] Eklund P, Kerdsongpanya S, Alling B (2016) Transition-metal-nitride-based thin films as novel energy harvesting materials. J Mater Chem C 4:3905–3914

[8] Biswas B, Saha B (2019) Development of semiconducting ScN. Phys Rev Mater 3:020301

[9] Maurya KC, Biswas B, Garbrecht M, Saha B (2019) Wave-vector dependent Raman scattering from coupled plasmon-LO phonons in epitaxial n-type ScN thin films. Phys Status Solidi Rapid Res Lett 13:1900196

[10] Nayak S, Baral M, Gupta M, Ganguly T, Shivaprasad SM, Saha B (2019) Rigid-band electronic structure of Scandium Nitride (ScN) across n-type to p-type carrier transition regime. Phys Rev B 99:161117(R)

[11] Rao D et al (2020) High mobility and high thermoelectric power factor in epitaxial ScN thin films deposited with plasma-assisted molecular beam epitaxy. Appl Phys Lett 116:152103

[12] Kerdsongpanya S, Nong NV, Pryds N, Žukauskaitė A, Jensen J, Birch J, Lu J, Hultman L, Wingqvist G, Eklund P (2011) Anomalously high thermoelectric power factor in epitaxial ScN thin films. Appl Phys Lett 99:232113

[13] Burmistrova PV, Zakharov DN, Favaloro T, Mohammed A, Stach EA, Shakouri A, Sands TD (2015) Effect of deposition pressure on the microstructure and thermoelectric properties of epitaxial ScN(001) thin films sputtered onto MgO(001) substrates. J Mater Res 30:626–634

[14] Saha B, Naik G, Drachev V, Boltasseva A, Marinero EE, Sands TD (2013) Electronic and optical properties of ScN and (Sc, Mn)N thin films deposited by reactive DC-magnetron sputtering. J Appl Phys 114:063519

[15] Saha B, Garbrecht M, Perez-Taborda JA, Fawey MH, Koh YR, Shakouri A, Martin-Gonzalez M, Hultman L, Sands TD (2017) Compensation of native donor doping in ScN: carrier concentration control and p-type ScN. Appl Phys Lett 110:252104

[16] Burmistrova PV, Maassen J, Favaloro T, Saha B, Salamat S, Koh YR, Lundstrom MS, Shakouri A, Sands TD (2013) Thermoelectric properties of epitaxial ScN films deposited by reactive magnetron sputtering onto MgO(001) substrates. J Appl Phys 113:153704

[17] King SW, Davis RF, Nemanich RJ (2014) Gas source molecular beam epitaxy of scandium nitride on silicon carbide and gallium nitride surfaces. J Vac Sci Technol A 32:061504

[18] Kerdsongpanya S, Sun B, Eriksson F, Jensen J, Lu J, Koh YK, Nong NV, Balke B, Alling B, Eklund P (2016) Experimental and theoretical investigation of $Cr_{1-x}Sc_xN$ solid solutions for thermoelectrics. J Appl Phys 120:215103

[19] Kerdsongpanya S, Hellman O, Sun B, Koh YK, Lu J, Nong NV, Simak SI, Alling B, Eklund P (2017) Phonon thermal conductivity of Scandium Nitride for thermoelectrics from first-principles calculations and thin-film growth. Phys Rev B 96:195417

[20] Alling B (2014) Metal to semiconductor transition and phase stability of $Ti_{1-x}Mg_xNy$ alloys investigated by first-principles calculations. Phys Rev B 89:085112

[21] Heyd J, Scuseria GE, Ernzerhof M (2003) Hybrid functionals based on a screened Coulomb potential. J Chem Phys 118:8207–8215

[22] Irokawa Y, Usami M (2016) First-principles calculations of semiconducting $TiMgN_2$. Jpn J Appl Phys 55:098001

[23] Baiwei B, Gall D (2018) A new semiconductor: $Ti_{0.5}$-$Mg_{0.5}N$(001). IEEE Nanotechnology Symposium (ANTS).

[24] Wang B, Kerdsongpanya S, McGahay ME, Milosevic E, Patsalas P, Gall D (2018) Growth and properties of epitaxial $Ti_{1-x}Mg_xN$(001) layers. J Vac Sci Technol A 36:061501.

[25] Gharavi MA (2019) Doctoral thesis titled: "Theoretical and Experimental Studies on Early Transition Metal Nitrides for Thermoelectrics" Linköping University LiU tryk.

[26] Kim J et al (2020) Influence of hydrogen and oxygen on the structure and properties of sputtered magnesium zirconium oxynitride thin films. J Mater Chem A 8:9364–9372.

[27] Gharavi MA, Armiento R, Alling B, Eklund P (2018) Theoretical study of phase stability, crystal and electronic structure of $MeMgN_2$ (Me = Ti, Zr, Hf) compounds. J Mater Sci 53:4294–4305. https://doi.org/10.1007/s10853-017-1849-0

[28] Bauers SR, Hamann DM, Patterson A, Perkins JD, Talley TR, Zakutayev A (2019) Composition, structure, and semiconducting properties of $Mg_xZr_{2-x}N_2$ thin films. Jpn J Appl Phys 58:SC1015.

[29] Hohenberg P, Kohn W (1964) Inhomogeneous Electron Gas. Phys Rev 136:B864–871

[30] Kohn W, Sham LJ (1965) Self-consistent equations including exchange and correlation effects. Phys Rev 140:A1133–1138

[31] Blöchl PE (1994) Projector augmented-wave method. Phys Rev B 50:17953–17979

[32] Kresse G, Hafner J (1993) Ab initio molecular dynamics for open-shell transition metals. Phys Rev B 48:13115–13118

[33] Kresse G, Furthmüller J (1996) Efficient iterative schemes for ab initio total-energy calculations using a plane-wave basis set. Phys Rev B 54:11169–11186

[34] Kresse G, Joubert D (1999) From ultrasoft pseudopotentials to the projector augmented-wave method. Phys Rev B 59:1758–1775

[35] Perdew JP, Burke K, Ernzerhof M (1996) Generalized gradient approximation made simple. Phys Rev Lett 77:3865–3868

[36] Zunger A, Wei SH, Ferreira LG, Bernard JE (1990) Special quasirandom structures. Phys Rev Lett 65:353–356

[37] Alling B, Höglund C, Hall-Wilton R, Hultman L (2011) Mixing thermodynamics of $TM_{1-x}Gd_xN$ (TM=Ti, Zr, Hf) from first principles. Appl Phys Lett 98:241911

[38] Armiento R et al. (2012–2017) The High-Throughput Toolkit (httk). https://httk.openmaterialsdb.se/

[39] Momma K, Izumi F (2011) *VESTA 3* for three-dimensional visualization of crystal, volumetric and morphology data. J Appl Crystallogr 44:1272–1276

[40] Wang L, Maxisch T, Ceder G (2006) Oxidation energies of transition metal oxides within the GGA+U framework. Phys Rev B 73:195107

[41] Jain A, Hautier G, Moore CJ, Ong SP, Fischer CC, Mueller T, Persson KA, Ceder G (2011) A high-throughput infrastructure for density functional theory calculations. Comp Mater Sci 50:2295–2310

[42] Monkhorst HJ, Pack JD (1976) Special points for Brillouin-zone integrations. Phys Rev B 13:5188–5192

[43] Droghetti A, Baadji N, Sanvito S (2009) MgN: a possible material for spintronic applications. Phys Rev B 80:235310

[44] Madsen GKH, Singh DJ, Boltz TraP (2006) A code for calculating band-structure dependent quantities. Comput Phys Commun 175:67–71.

[45] Jain A, Ong SP, Hautier G, Chen W, Richards WD, Dacek S, Cholia S, Gunter D, Skinner D, Ceder G, Persson KA (2013) The materials project: a materials genome approach to accelerating materials innovation. APL Mater 1:011002

[46] Goldsmid HJ (2010) Introduction to thermoelectricity. Springer, Heidelberg.

[47] Shakouri A (2011) Recent developments in semiconductor thermoelectric physics and materials. Annu Rev Mater Res 41:399–431

[48] Bauers SR et al (2019) Ternary nitride semiconductors in the rocksalt crystal structure. PNAS 116:14829–14834

[49] Bauers SR et al (2020) Epitaxial growth of rock salt $MgZrN_2$ semiconductors on MgO and GaN. Appl Phys Lett 116:102102

[50] Blanton EW, He K, Shan J, Kash K (2017) Characterization and control of $ZnGeN_2$ cation lattice ordering. J Cryst Growth 461:38–45